

# Embodied Executable Policy Learning with Language-based Scene Summarization

Jielin Qiu<sup>1,2\*</sup>, Mengdi Xu<sup>1,\*</sup>, William Han<sup>1,\*</sup>, Seungwhan Moon<sup>2</sup>, Ding Zhao<sup>1</sup>

<sup>1</sup>Carnegie Mellon University, <sup>2</sup>Meta Reality Labs

{jieling, mengdixu, wjhan, dingzhao}@andrew.cmu.edu, shanemoon@meta.com

## Abstract

Large Language models (LLMs) have shown remarkable success in assisting robot learning tasks, i.e., complex household planning. However, the performance of pretrained LLMs heavily relies on domain-specific templated text data, which may be infeasible in real-world robot learning tasks with image-based observations. Moreover, existing LLMs with text inputs lack the capability to evolve with non-expert interactions with environments. In this work, we introduce a novel learning paradigm that generates robots' executable actions in the form of text, derived solely from visual observations. Our proposed paradigm stands apart from previous works, which utilized either language instructions or a combination of language and visual data as inputs. We demonstrate that our proposed method can employ two fine-tuning strategies, including imitation learning and reinforcement learning approaches, to adapt to the target test tasks effectively. We conduct extensive experiments involving various model selections, environments, and tasks across 7 house layouts in the VirtualHome environment. Our experimental results demonstrate that our method surpasses existing baselines, confirming the effectiveness of this novel learning paradigm.

## 1 Introduction

There has been a surge of interest in building Large Language Models (LLMs) pretrained on large-scale datasets and exploring LLMs' capability in various downstream tasks. LLMs start from the Transformer model (Vaswani et al., 2017b) and are first developed to solve different natural language processing (NLP) applications (Devlin et al., 2019; Liu et al., 2019; Brown et al., 2020). Recently, LLMs have also shown great potential for accelerating learning in many other domains by generating learned embeddings as meaningful representations

for downstream tasks and encoding transferable knowledge in large pretraining datasets.

In this paper, we focus on the problem of facilitating robot learning by having a LLM in the loop. The robot generates actions according to its environment observations, which are, in general, sensory information in the format of images, point clouds, or kinematic states. We identify one key challenge in massively deploying LLMs to assist robots is that *LLMs lack the capability to understand such non-text-based environment observations*. To solve this challenge, Liang et al. (2022) utilize rule-based perception APIs to transform image-based observations into text formats, which then serve as inputs to the LLM. We instead propose to integrate the multimodal learning paradigm to transform images into texts, which allows more principled and efficient transfer to novel robot learning tasks than rule-based APIs. Another key challenge is *the widely-existing large distribution shifts between the training tasks of large pretrained models and testing tasks in the domain of robot learning*. To close the domain gap, Li et al. (2022b) adapt the pretrained LLM to downstream tasks via finetuning with observations converted into text descriptions. In the presence of realistic visual observations, an appropriate method to co-adapt pretrained foundation models for testing tasks in robot learning is still being determined.

To address the above challenges, we propose a new visual-based robot learning paradigm that takes advantage of embedded knowledge in both multimodal models and LLMs. To align different modalities in the visual observations and text-based actions, we consider language as the bridge information. We build a scene-understanding model (SUM) with a pretrained image captioning model to grant the robot the ability to describe the surrounding environment with natural language. We then build an action prediction model (APM) with a LLM to generate execution actions according

\* Equal contribution

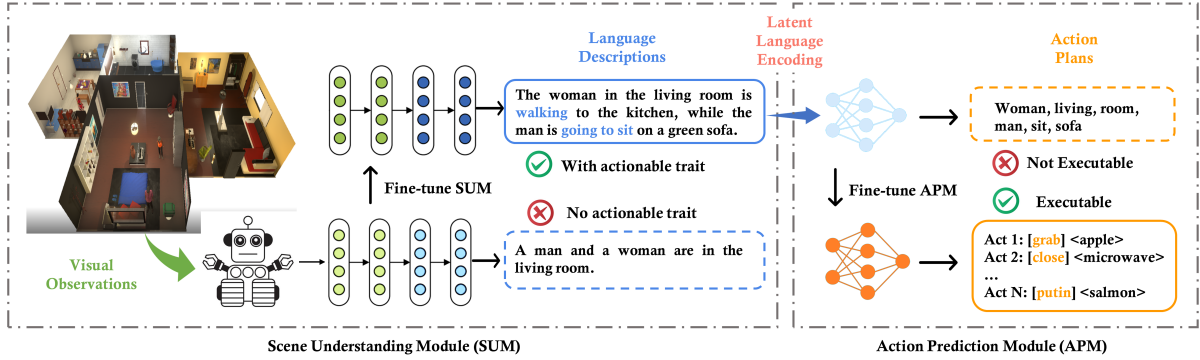


Figure 1: The overall architecture of our approach, which includes a scene understanding module (SUM) and an action prediction module (APM). The agent takes pure visual observations and encodes the information as latent language, then the language is transferred to APM for action generation. APM fine-tuned on VirtualHome can generate executable action plans directly.

to the scene caption in the format of natural language. To adapt pretrained models in SUM and APM to downstream robot learning tasks, we propose to finetune the multimodal model in SUM with pre-collected domain-specific image-caption pairs and the language model in APM with corresponding language-action pairs. Besides finetuning with expert demonstrations, we further propose a finetuning paradigm of APM based on the sparse environment feedback to endow APM’s capability to evolve with non-expert data. An illustration of the proposed framework is Figure 1.

Our contributions are summarised as follows:

- We introduce a novel robot learning paradigm with LLM in the loop that handles multiple modalities of visual observations and text-based actions in a principled manner. We bridge both modalities with natural language generated by a pretrained multimodal model.
- To adapt to target testing tasks, we propose two fine-tuning strategies, including imitation learning and reinforcement learning approaches. We collect a new expert dataset for imitation learning-based finetuning.
- We test the adaptation performance of multiple models of SUM and APM in seven house layouts in the VirtualHome environment. Our experiments demonstrate that our proposed paradigm shows promising results.

## 2 Related Work

**Language Models in Robot Learning** Recently, several works have successfully combined LLMs with robot learning by taking advantage of the knowledge learned by LLMs i.e., reasoning (Liang et al., 2022; Zeng et al., 2022; Zellers et al., 2021), planning (Shah et al., 2022; Huang et al., 2022b;

Kant et al., 2022; Li et al., 2022b; Huang et al., 2022a), manipulation (Shafiullah et al., 2022; Jiang et al., 2022; Shridhar et al., 2022; Bucker et al., 2022; Ren et al., 2022; Tam et al., 2022; Khandelwal et al., 2022; Shridhar et al., 2021; Xu et al., 2022, 2023), and navigation (Lin et al., 2022; Parisi et al., 2022; Gadre et al., 2022; Hong et al., 2021; Majumdar et al., 2020), which demonstrated the feasibility of using LLM to assist robot learning.

**Visual Feedback in Robot Learning** Visual feedback is commonly used in robot learning. Gothoskar et al. (2020) learned a generative model from actions to image observations of features to control a robot from visual feedback. Ma et al. (2022) proposed a self-supervised pretrained visual representation model which is capable of generating dense and smooth reward functions for unseen robotic tasks. Strokinina et al. (2022) reviewed the methods of reward estimation and visual representations used in learning-based approaches for robotics applications. Mohtasib et al. (2021) studied the performance of dense, sparse, visually dense, and visually sparse rewards in deep RL. Kurita and Cho (2020) proposed the direct navigation approach based on an image captioning model. Li et al. (2019) combined image captioning models and planning models, but Li et al. (2019) took pure language instructions as input, while our approach takes pure visual observations as input.

**Pre-training and Fine-tuning of Language Models** Over the past few years, fine-tuning (Howard and Ruder, 2018) has superseded the use of feature extraction of pretrained embeddings (Peters et al., 2018) while pretrained language models are favored over models trained on many tasks due to their increased sample efficiency and performance (Ruder, 2021). The success of these methods has

led to the development of even larger models (Devlin et al., 2019; Raffel et al., 2019). Fine-tuning pretrained contextual word embedding models to supervised downstream tasks has become commonplace (Hendrycks et al., 2020; Dodge et al., 2020). Zeng et al. (2022) examined the sampling effects in reinforcement learning with GPT and BERT. More related works can be found in Appendix A.

### 3 Method

In this section, we first introduce our focused problem in Section 3.1, which is generating a visual-based policy by leveraging pretrained large models. We then introduce SUM, which learns language descriptions of the surrounding environment in Section 3.1, and APM which predicts actions based on SUM’s caption output in 3.2. To grant both SUM and APM the capability of making the correct understanding and decision in the target domain, we propose finetuning algorithms in Section 3.1 and 3.2. Our code and data are provided in the supplementary materials.

#### 3.1 Problem Formulation

We consider a general and realistic robot learning task where a robot agent receives a sequential visual observation  $V = [v_1, v_2, \dots, v_t]$ , where  $t$  is the timestep, and aims to generate a sequence of actions  $A = [a_1, a_2, \dots, a_t]$  based on the pure visual observations  $V$ . Traditionally, the robot’s policy is trained from scratch in the target tasks. Inspired by the success of large pretrained models, we aim to explore the benefit of utilizing pretrained LLMs and multimodal models for general robot learning tasks, where only visual observations are available as inputs. Given the prevailing domain shift between the training domain of the pretrained models and the robot learning tasks, we are motivated to develop a principled finetuning method.

**SUM: Learning Scene Descriptions from Visual Observations into Language.** The goal of the SUM (scene understanding module) is to transform visual observations into language descriptions that contain an actionable trait to it. SUM shares similar functionalities of visual captioning models, which aim to automatically generate fluent and informative language descriptions of an image (Ke et al., 2019). For the SUM to be capable of providing scene descriptions from visual observations, it needs to distill representative and meaningful visual representations from an image, then generate

coherent and intelligent language descriptions. In our framework, we adopt models with image captioning ability as our SUM, such as OFA (Wang et al., 2022), BLIP (Li et al., 2022a), and GRIT (Nguyen et al., 2022). We will discuss the details of possible image captioning models to use in Section 4. Generally, image captioning models employ a visual understanding system and a language model capable of generating meaningful and syntactically correct captions (Stefanini et al., 2021). In a standard configuration, the task can be defined as an image-to-sequence problem, where the inputs are pixels, which will be encoded as one or multiple feature vectors in the visual encoding step. The language model will take the information to produce a sequence of words or subwords decoded according to a given vocabulary in a generative way.

With the development of self-attention (Vaswani et al., 2017a), the visual features achieved remarkable performance due to multimodal pretraining and early-fusion strategies (Tan and Bansal, 2019; Lu et al., 2019; Li et al., 2020; Zhou et al., 2019). As for language models, the goal is to predict the probability of a given sequence of words occurring in a sentence. As such, it is a crucial component in image captioning, as it gives the ability to deal with natural language as a stochastic process. Formally, given a sequence of  $n$  words  $y_1, \dots, y_n$ , the language model component of an image captioning algorithm assigns a probability  $P(y_1, y_2, \dots, y_n | \mathbf{X})$  to the sequence as:

$$P(y_1, y_2, \dots, y_n | \mathbf{X}) = \prod_{i=1}^n P(y_i | y_1, y_2, \dots, y_{i-1}, \mathbf{X}) \quad (1)$$

where  $\mathbf{X}$  represents the visual encoding on which the language model is specifically conditioned. Notably, when predicting the next word given the previous ones, the language model is autoregressive, which means that each predicted word is conditioned on the previous ones. Additionally, the language model usually decides when to stop generating captions by outputting a special end-of-sequence token.

#### 3.2 APM: Decoding Language Information into Executable Action Plans

The goal of APM (action prediction module) is to transform latent language information from the SUM output into executable action plans. Since both latent language information and executable action plans are sequential data, a LLM with encoder-

decoder architecture is a good option for APM in our framework. In addition, a LLM pretrained on a vast corpus of text already has adequate knowledge, which can be fine-tuned on other tasks to improve learning efficiency.

A LLM with encoder-decoder architecture suits well for our setting. The encoder is responsible for reading and understanding the input language information from SUM, which is usually based on transformer architecture, and creates a fixed-length vector representation, called the context vector. The decoder then takes the context vector as input and generates the output, in our case, the executable action plans. The decoder uses the context vector to guide its generation of the output and make sure it is coherent and consistent with the input information. However, due to the distribution change between the data that LLM was pretrained on and the new task, the LLM needs to be fine-tuned on the task-specific data to transfer the knowledge. The fine-tuning strategies will be introduced in the following sections. For our LLMs, we use well-adopted pretrained architectures, including BERT (Devlin et al., 2019), RoBERTa (Liu et al., 2019), and BART (Lewis et al., 2020), as both the encoder and decoder. The goal of the LLM is to learn how to generate programmable, executable actions from the language descriptions outputted by SUM.

### 3.3 Training Pipeline

The training pipeline contains two steps. We first fine-tune SUM with the curated VirtualHome observations (More details about data collection are introduced in Section 4.2). This fine-tuning step is to familiarize SUM with the types of scenes present in the task-specific data. We present pseudocode to fine-tune the SUM in Algorithm 1 in Appendix C.

In the second stage, we load the fine-tuned SUM and encode the outputs as latent language embeddings. The embeddings are then fed into the APM, which is then fine-tuned using different fine-tuning loss objectives (supervised one or policy gradient, more details are introduced in Section 4), to achieve the optimal policy with maximum rewards. The pseudocode for finetuning APM with IL and REINFORCE are in Algorithms 2 and 3 in Appendix C, respectively.

### 3.4 Fine-tuning APM with IL and RL

For LLM, the output word is sampled from a learned distribution over the vocabulary words. In the most simple scenario, i.e. the greedy decoding

mechanism, the word with the highest probability is output. The main drawback of this setting is that possible prediction errors quickly accumulate along the way. To alleviate this drawback, one effective strategy is to use the beam search algorithm (Cho et al., 2014; Koehn, 2007) that, instead of outputting the word with maximum probability at each time step, maintaining  $k$  sequence candidates and finally outputs the most probable one. For the training or fine-tuning strategies, most strategies are based on cross-entropy (CE) loss and masked language model (MLM). But recently, RL-based learning objective has also been explored, which allows optimizing for captioning-specific non-differentiable metrics directly.

#### Imitation Learning with Cross-Entropy Loss

CE loss aims to minimize negative log-likelihood of the current word given the previous ground-truth words at each timestep. Given a sequence of target words  $y_{1:T}$ , the loss is defined as:

$$L_{XE}(\theta) = - \sum_{i=1}^n \log(P(y_i | y_{1:i-1}, \mathbf{X})) \quad (2)$$

where  $P$  is the probability distribution induced by LLM,  $y_i$  the ground-truth word at time  $i$ ,  $y_{1:i-1}$  indicate the previous ground-truth words, and  $\mathbf{X}$  the visual encoding. The cross-entropy loss is designed to operate at the word level and optimize the probability of each word in the ground-truth sequence without considering longer-range dependencies between generated words. The traditional training setting with cross-entropy also suffers from the exposure bias problem (Ranzato et al., 2015) caused by the discrepancy between the training data distribution as opposed to the distribution of its own predicted words.

#### Reinforcement Learning with REINFORCE

Given the limitations of word-level training strategies observed when using limited amounts of data, a significant improvement was achieved by applying the RL approach. Under this setting, the LLM is considered as an agent whose parameters determine a policy. At each time step, the agent executes the policy to choose an action, i.e. the prediction of the next word in the generated sentence. Once the end-of-sequence is reached, the agent receives a reward, and the aim of the training is to optimize the agent parameters to maximize the expected reward (Stefanini et al., 2021).

Similar to Ranzato et al. (2015), for our policy gradient method, we use REINFORCE (Williams,



1992; Sutton et al., 1999), which uses the full trajectory, making it a Monte-Carlo method, to sample episodes to update the policy parameter. For fine-tuning LLMs using RL, we need to frame the problem into an Agent-Environment setting where the agent (policy) can interact with the environment to get the reward for its actions. This reward is then used as feedback to train the model. The mapping of the entities is from the agent (policy), which is an LLM, and the environment (the reward function, also named the model), which generates rewards. The reward function consumes the input as well as the output of the LLM to generate the reward. The reward is then used in a loss function, and the policy is updated. Formally, to compute the loss gradient, beam search and greedy decoding are leveraged as follows:

$$\nabla_{\theta} L(\theta) = -\frac{1}{k} \sum_{i=1}^k \left( (r(\mathbf{w}^i) - b) \nabla_{\theta} \log P(\mathbf{w}^i) \right) \quad (3)$$

where  $\mathbf{w}^i$  is the  $i$ -th sentence in the beam or a sampled collection,  $r(\cdot)$  is the reward function, and  $b$  is the baseline, computed as the reward of the sentence obtained via greedy decoding (Rennie et al., 2016), or as the average reward of the beam candidates (Cornia et al., 2019). Note that, since it would be difficult for a random policy to improve in an acceptable amount of time, the usual procedure entails pretraining with cross-entropy or masked language model first, and then fine-tuning stage with RL by employing a sequence level metric as the reward. This ensures the initial RL policy is more suitable than the random one.

## 4 Experiments

This section introduces the environment we used in the experiments, the experimental settings, evaluations, and results. We would like to answer the following questions with experiments: (1) Can the proposed paradigm take pure visual observations to generate executable robot actions; (2) What kinds of SUM are able to provide better scene descriptions for robot learning; (3) What kinds of APM show better action decoding ability in generating executable actions; (4) What kinds of fine-tuning strategies show better performance under this setting; (5) Can the model achieve consistent performance across different environments?

### 4.1 Environments and Metrics

**Environments** We build the experiment environments based on VirtualHome (Puig et al., 2018a;

Liao et al., 2019), a multi-agent, virtual platform for simulating daily household activities. (Puig et al., 2018b). Puig et al. (2018a) provides a dataset of possible tasks in their respective environments. Each task includes a natural language description of the task ("Put groceries in the fridge."), an elongated and more detailed natural language description of the task ("I put my groceries into the fridge."), and the executable actions to perform the task in VirtualHome ([[Walk] < groceries > (1), [Grab] < groceries > (1), ... [Close] < fridge > (1)]). We define the training and testing tasks based on the natural language descriptions of the task due to their straightforwardness.

In VirtualHome, the agents are represented as 3D humanoid avatars that interact with given environments through provided, high-level instructions. Puig et al. (2018a) accumulated a knowledge base of instructions by using human annotators from AMT to first yield verbal descriptions of verbal activities. These descriptions were further translated by AMT annotators into programs utilizing a graphical programming language, thus amassing around 3,000 household activities in 50 different environments (Puig et al., 2018a). In this study, we evaluate our model’s performance in 7 unique environments, which are shown in Figure 4 in the Appendix. Each environment has a distinctive set of objects and actions that may be interacted with by agents.

**Metrics** We used standard NLP evaluation metrics, i.e., BLEU (Papineni et al., 2002), ROUGE (Lin, 2004), METEOR (Banerjee and Lavie, 2005), CIDEr (Vedantam et al., 2015), and SPICE (Anderson et al., 2016), for evaluating LLMs. In addition, we introduced the execution rate following Li et al. (2022b). The execution rate is defined as the probability of the agent’s success in performing the outputted action from APM over the whole trajectory. More experimental setup details about SUM and APM are listed in Appendix D. We run 10 seeds for each environment.

### 4.2 Datasets

To fine-tune SUM and APM on task-specific robot learning scenarios, we collect data via VirtualHome, including the agent’s observations, language instructions, and action sequences. During data collection, a household activity program can be described as: [[action<sub>*i*</sub>] < object<sub>*i*</sub> > (id<sub>*i*</sub>), ... [action<sub>*n*</sub>] < object<sub>*n*</sub> > (id<sub>*n*</sub>)], where  $i$  denotes

each step of the program,  $action_i$  and  $object_i$  denotes the action performed on the object at step  $i$ , and  $id_i$  symbolizes the unique identifier of  $object_i$  (Puig et al., 2018a). The original dataset was augmented by ResActGraph (Liao et al., 2019). After augmentation, the dataset contains over 30,000 executable programs, with each environment containing over 300 objects and 4,000 spatial relations. Additionally, we collect the image and text pairs separated by the environments they were executed in. This is important due to the different objects and actions available in each environment. However, as noted in Puig et al. (2018a) and Liao et al. (2019), not all programs were executable.

During data collection, we observed that the text was comprised of two words (e.g., walking bathroom, sitting chair, etc). To have a robust text description, we prompt engineered the texts with a fill-mask pipeline using BERT (Devlin et al., 2019; Song et al., 2019). For this study, we collect programs executed in three different views: ‘AUTO’, ‘FIRST\_PERSON’, and ‘FRONT\_PERSON’ as shown in Figure 3 in Appendix B. In the ‘AUTO’ view, there are locked cameras in every scene through which the program randomly iterates through. The ‘FIRST\_PERSON’ view observes the agent’s actions through the first-person point of view. The ‘FRONT\_PERSON’ view monitors the agent’s actions through the front in a locked third-person point of view. Therefore, the final count of image-text pairs for our dataset in the ‘AUTO’, ‘FIRST\_PERSON’, and ‘FRONT\_PERSON’ views are 26,600, 26,607, and 26,608, respectively. More details can be found in Appendix B.

### 4.3 Experimental Setup

**SUM Setting** For SUM, we use the following image captioning models to serve as SUM: OFA (Wang et al., 2022), BLIP (Li et al., 2022a), and GRIT (Nguyen et al., 2022). Both OFA and BLIP are pretrained on the same five datasets, while the GRIT model (Nguyen et al., 2022) is pretrained on a different combination of datasets. For OFA, we adopted OFA<sub>Large</sub> due to its superior performance in five variations. OFA<sub>Large</sub> wields ResNet152 (He et al., 2015) modules with 472M parameters and 12 encoders and decoder layers. For BLIP, we used ViT-L/16 as the image encoder due to its better performance. For GRIP, we follow Nguyen et al. (2022) which utilizes the Deformable DETR (Zhu

et al., 2020) framework. Note that in our study we want SUM to generate captions that not only describe the scene but also try to derive action from it. We observe that adding the prompt "a picture of " following Wang et al. (2021) causes the model to be biased in solely describing the scene, which would in turn not be helpful for generating actionable captions. Therefore, we remove prompts in the SUM setting. We load pretrained models and fine-tune them for 7 epochs on our collected VirtualHome dataset. We keep the hyper-parameters consistent with the original implementations (Li et al., 2022a; Wang et al., 2022; Nguyen et al., 2022).

**APM Setting** We take LLM to act as our APM. The goal of APM is to generate executable programs for the VirtualHome simulator. We deem the program outputted by the APM executable if the agent in the VirtualHome simulator is able to understand and perform the action. When the action is executed by the agent, the simulator is then directed to output images and captions that are synonymous with the input of SUM. The output hidden layers of SUM acts as the input embeddings to the APM, while the tokenized executable actions act as labels. The last hidden layer of APM acts as input embeddings for the tokenizer and generates token identifiers. The token identifiers are finally decoded into programmable actions.

## 5 Results and Discussions

### 5.1 Model Performance with IL Fine-tuning

We first want to show the benefit of the proposed framework compared with other model architectures. Concretely, in the IL setting with expert data, we compare the execution rate of our model with the MLP, MLP-1 and LSTM baselines in Li et al. (2022b). Our model has OFA in SUM and BART as APM. Note that all the baselines are not trained by datasets in other domains and have structured text input instead of realistic visual inputs as our proposed model. In the LSTM baseline, the hidden representation from the last timestep, together with the goal and current observation, are used to predict the next action. MLP and MLP-1 both take the goal, histories, and the current observation as input and send them to MLPs to predict actions. MLP-1 has three more average-pooling layers than MLP that average the features of tokens in the goal, history actions, and the current observation, respectively, before sending them to the MLP layer. More details about the baselines can be found in

Table 1: Results by different SUM fine-tuned by imitation learning (IL) objective, where BERT serves as APM. The results are shown on 7 different environments in VirtualHome and also the average performance. The best result in each environment and each SUM model is marked in black and bold. The best SUM result with the highest average performance across 7 environments is marked in orange and bold.

| SUM/Results(%)             | Environment | Bleu-1           | Bleu-2           | Bleu-3           | Bleu-4           | ROUGE-L          | METEOR           | CIDEr             | SPICE            | Execution Rate   |
|----------------------------|-------------|------------------|------------------|------------------|------------------|------------------|------------------|-------------------|------------------|------------------|
| OFA (Wang et al., 2022)    | 1           | 55.1±0.05        | 45.4±0.10        | 36.5±0.20        | 23.0±0.00        | 60.0±0.16        | 33.4±0.00        | 30.2±0.44         | <b>49.9±0.43</b> | 78.0±2.39        |
|                            | 2           | 58.0±0.20        | 41.7±0.19        | 35.1±1.01        | 22.1±0.73        | 60.1±0.50        | 34.1±0.52        | 30.3±0.71         | 48.1±0.41        | 79.9±2.37        |
|                            | 3           | 55.3±0.30        | 42.3±0.62        | 34.9±0.15        | 23.0±0.00        | 60.5±0.01        | 34.8±0.64        | 31.2±0.55         | 48.4±0.17        | 80.0±3.29        |
|                            | 4           | 57.8±0.73        | 42.2±0.31        | 35.3±0.38        | 24.5±0.67        | 59.9±0.45        | 34.6±0.54        | 33.1±0.63         | 49.0±0.66        | 79.9±4.14        |
|                            | 5           | 59.4±0.44        | 40.3±0.03        | 34.8±0.02        | 24.2±0.37        | 59.7±0.25        | 35.1±0.62        | 32.7±0.24         | 38.0±0.13        | 77.4±1.12        |
|                            | 6           | <b>60.5±0.01</b> | <b>48.1±0.53</b> | <b>36.6±0.07</b> | <b>25.1±0.15</b> | <b>61.9±0.13</b> | <b>36.2±0.60</b> | <b>34.6±1.07</b>  | <b>49.9±0.77</b> | <b>80.5±1.13</b> |
|                            | 7           | 58.2±0.30        | 46.5±0.58        | 34.6±0.04        | 22.3±0.08        | 58.3±0.92        | 35.6±0.62        | 30.8±0.37         | 44.2±0.33        | 69.2±2.31        |
|                            | Average     | <b>57.8±0.92</b> | <b>43.8±1.02</b> | <b>35.4±0.63</b> | <b>23.5±0.77</b> | <b>60.1±0.41</b> | <b>34.8±0.62</b> | <b>31.8±1.31</b>  | <b>46.8±0.80</b> | <b>77.8±3.26</b> |
| BLIP (Li et al., 2022a)    | 1           | 51.1±0.50        | 42.6±0.41        | 33.2±0.34        | 21.1±0.63        | 60.8±0.73        | 34.7±0.63        | <b>35.5±00.09</b> | 42.7±0.91        | 72.6±1.99        |
|                            | 2           | 50.5±0.87        | 41.8±0.72        | 30.5±28          | 22.3±0.34        | 60.3±0.64        | 33.6±0.87        | 30.0±0.72         | 42.8±0.99        | 66.1±4.21        |
|                            | 3           | 52.4±0.54        | 43.2±0.65        | 33.6±0.13        | 21.1±0.52        | 61.4±0.29        | 34.5±0.12        | 31.1±0.00         | <b>48.9±0.80</b> | 85.0±3.32        |
|                            | 4           | 51.0±1.19        | 42.1±0.87        | <b>33.8±0.54</b> | 22.8±0.65        | 60.6±0.76        | 34.4±0.98        | 35.1±0.85         | 46.0±0.74        | 73.0±3.65        |
|                            | 5           | 49.0±0.53        | 38.8±0.43        | 30.4±0.72        | 20.0±0.47        | 58.6±0.65        | 34.1±0.75        | 21.0±0.66         | 30.8±0.69        | 67.2±0.93        |
|                            | 6           | <b>52.6±0.79</b> | <b>44.5±0.00</b> | 31.0±0.63        | <b>24.8±0.62</b> | <b>62.0±0.73</b> | <b>35.3±1.02</b> | 31.0±0.02         | 42.4±0.87        | 84.1±3.54        |
|                            | 7           | 52.7±0.50        | 44.0±0.21        | 33.6±0.18        | 24.0±0.52        | 61.7±0.08        | 34.5±0.60        | 34.5±0.81         | 48.8±0.28        | <b>86.0±4.92</b> |
|                            | Average     | 51.3±0.31        | 42.4±0.54        | 32.3±0.66        | 22.3±0.31        | 60.7±0.63        | 34.4±0.75        | 31.2±0.87         | 43.2±0.97        | 76.3±5.22        |
| GRIT (Nguyen et al., 2022) | 1           | 50.5±0.99        | 40.5±0.86        | 31.8±1.82        | 20.7±1.02        | 60.0±1.44        | 33.1±0.97        | 30.4±1.42         | 41.7±0.85        | 69.2±5.57        |
|                            | 2           | 52.1±0.66        | 41.8±1.77        | 31.7±1.92        | 20.1±0.97        | 59.9±0.65        | 32.1±0.76        | 29.4±0.87         | 42.0±0.88        | 71.4±5.52        |
|                            | 3           | 52.3±0.88        | 40.3±0.82        | 32.1±0.77        | 19.9±1.53        | 60.4±0.68        | 31.7±0.66        | 30.1±2.52         | 43.5±1.64        | 71.3±5.98        |
|                            | 4           | 51.9±0.93        | 39.8±0.92        | 31.8±0.97        | 21.3±1.72        | 59.7±1.22        | 32.0±0.76        | 30.0±0.79         | 42.8±0.84        | 72.8±4.65        |
|                            | 5           | <b>54.7±0.93</b> | 42.3±1.02        | 33.2±1.25        | 24.5±0.93        | 62.3±1.42        | <b>33.8±1.77</b> | 30.7±1.32         | <b>44.6±1.23</b> | <b>78.5±5.07</b> |
|                            | 6           | 54.6±1.42        | <b>44.7±1.64</b> | <b>34.1±1.32</b> | <b>25.8±1.22</b> | <b>65.8±1.25</b> | 30.1±2.31        | <b>34.5±0.72</b>  | 44.0±0.96        | 78.4±3.66        |
|                            | 7           | 53.9±0.88        | 42.0±1.79        | 32.6±2.00        | 22.5±0.90        | 63.4±1.00        | 31.8±1.23        | 32.3±1.31         | 43.1±1.41        | 70.0±3.99        |
|                            | Average     | 52.9±0.18        | 41.6±0.87        | 32.4±0.72        | 22.1±0.68        | <b>61.6±0.53</b> | 32.1±0.33        | 31.1±0.25         | 43.1±0.76        | 73.1±3.11        |

Table 2: Results by different APM fine-tuned by imitation learning (IL) loss objective. The results are shown by the average of 7 different environments in VirtualHome. The best results are marked in bold.

| APM     | SUM  | Bleu-1           | Bleu-2           | Bleu-3           | Bleu-4           | ROUGE-L          | METEOR           | CIDEr            | SPICE            | Execution Rate   |
|---------|------|------------------|------------------|------------------|------------------|------------------|------------------|------------------|------------------|------------------|
| BERT    | OFA  | <b>57.8±0.92</b> | <b>43.8±1.02</b> | <b>35.4±0.63</b> | <b>23.5±0.77</b> | 60.1±0.41        | <b>34.8±0.62</b> | <b>31.8±1.31</b> | <b>46.8±0.80</b> | <b>77.8±3.26</b> |
|         | BLIP | 51.3±0.31        | 42.4±0.54        | 32.3±0.66        | 22.3±0.31        | 60.7±0.63        | 34.4±0.75        | 31.2±0.87        | 43.2±0.97        | 76.3±5.22        |
|         | GRIT | 52.9±0.18        | 41.6±0.87        | 32.4±0.72        | 22.1±0.68        | <b>61.6±0.53</b> | 32.1±0.33        | 31.1±0.25        | 43.1±0.76        | 73.1±3.11        |
| RoBERTa | OFA  | <b>57.7±0.01</b> | <b>43.2±0.00</b> | <b>35.6±0.48</b> | <b>24.1±0.36</b> | 59.9±0.26        | <b>34.7±0.51</b> | 31.4±0.47        | <b>47.3±0.38</b> | 75.4±3.86        |
|         | BLIP | 50.5±0.71        | 41.1±0.29        | 32.0±0.11        | 23.5±0.64        | <b>61.1±0.88</b> | 33.0±0.70        | <b>31.8±0.81</b> | 42.9±0.94        | <b>77.7±0.71</b> |
|         | GRIT | 53.1±1.02        | 42.0±0.90        | 34.1±1.01        | 23.1±1.22        | 60.4±1.92        | 31.5±0.59        | 31.5±1.42        | 42.8±1.77        | 75.4±4.39        |
| BART    | OFA  | <b>59.5±0.09</b> | <b>45.9±0.31</b> | <b>39.8±0.37</b> | <b>28.1±0.72</b> | 61.3±0.65        | <b>37.2±0.69</b> | <b>34.4±0.78</b> | <b>47.0±0.88</b> | <b>79.0±1.91</b> |
|         | BLIP | 52.9±0.80        | 44.3±0.52        | 35.5±0.49        | 25.3±0.62        | 62.2±1.12        | 35.3±1.62        | 32.0±0.97        | 44.5±0.88        | 76.0±1.98        |
|         | GRIT | 54.2±1.68        | 43.2±1.85        | 33.6±1.60        | 25.3±0.93        | <b>62.7±1.85</b> | 33.8±0.62        | 33.7±0.74        | 44.7±1.12        | 77.9±1.77        |

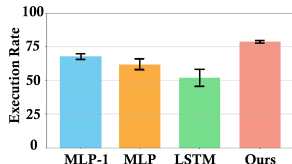


Figure 2: Comparison with baselines in the imitation learning setting evaluated by the execution rate.

Li et al. (2022b). As shown in Figure 2, our approach outperforms baselines in Li et al. (2022b) in terms of a higher average execution rate and a smaller standard deviation, though all the methods are trained on expert data with imitation learning objectives. The results show that the pretrained embeddings and large model architecture benefit the performance in downstream robot learning tasks.

## 5.2 Model Performance with RL Fine-tuning

We provide the model performance after fine-tuning SUM with a frozen BERT in Table 1 for the IL setting with expert data and in Table 3 for the RL setting. The results after fine-tuning APM with the fine-tuned SUM are shown in Table 2 and Table 4. We found that fine-tuning with expert data in IL results in higher average and per-environment per-

formance than fine-tuning with RL, which shows the benefit of having access to the expert datasets. However, fine-tuning with RL still brings performance improvement to 57.2% as in Table 4. Note that without finetuning, the outputs of the LLMs in APM are generally not executable as shown in Figure 1. Moreover, we consistently observe that the combination of having OFA in SUM and BART as APM achieves the best performance after both IL (Table 2) and RL (Table 4) fine-tuning.

## 5.3 Ablation Study

To deeply understand the importance of different components in our paradigm that affect the overall performance, we conduct ablation studies on different factors including different components in SUM, different components in APM, and different environment variations.

**Different Components in SUM** The performances of using different components in SUM for IL and RL fine-tuning are in Table 1 and Table 3, respectively. From Table 1, we see that with expert data, OFA achieves better results than BLIP and GRIT on the average performance over 7 environ-

Table 3: Execution Rates by different SUM fine-tuned by REINFORCE, where BERT serves as APM. The results are shown on 7 different environments and also the average performance. The best results are marked in bold.

| SUM                        | Env-1            | Env-2            | Env-3            | Env-4            | Env-5            | Env-6            | Env-7            | Average          |
|----------------------------|------------------|------------------|------------------|------------------|------------------|------------------|------------------|------------------|
| OFA (Wang et al., 2022)    | 50.1±0.65        | 50.3±0.52        | 51.5±0.48        | <b>57.8±0.88</b> | 55.2±0.00        | 56.6±0.37        | <b>59.3±0.48</b> | 54.4±0.55        |
| BLIP (Li et al., 2022a)    | <b>52.7±0.78</b> | <b>53.4±1.00</b> | <b>53.5±0.92</b> | 55.6±0.68        | <b>60.1±0.49</b> | <b>59.3±0.91</b> | 49.9±0.90        | <b>54.9±1.99</b> |
| GRIT (Nguyen et al., 2022) | 38.7±1.02        | 40.0±1.11        | 51.3±0.99        | 48.2±0.90        | 46.5±0.85        | 55.8±0.70        | 45.3±1.08        | 46.5±2.01        |

Table 4: Results by different APM fine-tuned by REINFORCE loss objective, averaging on 7 different environments. The best results are marked in bold.

| APM     | SUM  | Execution Rate (%) |
|---------|------|--------------------|
| BERT    | OFA  | <b>54.7±1.15</b>   |
|         | BLIP | 54.1±1.37          |
|         | GRIT | 53.9±3.00          |
| RoBERTa | OFA  | <b>55.6±4.31</b>   |
|         | BLIP | 55.2±1.16          |
|         | GRIT | 54.8±2.54          |
| BART    | OFA  | <b>57.2±2.43</b>   |
|         | BLIP | 57.0±3.12          |
|         | GRIT | 55.8±0.99          |

ments. We conjecture that this may be due to OFA being pretrained on 20M image-text pairs, which is larger than the size of other models’ pretraining data. While under REINFORCE fine-tuning loss, as in Table 3, BLIP slightly outperforms OFA in terms of average performance but has around 4 times larger standard deviation than OFA.

**How Visual Observations Affect SUM** Visual observation quality is vital for SUM. In FIRST\_PERSON view, which lacks explicit action portrayal, SUM faces challenges in generating high-quality textual descriptions. Complex visual scenarios, like blank walls or cluttered scenes with numerous objects, also impede SUM’s ability to provide informative descriptions matching the action or task at hand.

**Different Components in APM** The results of using different components in APM for IL and RL fine-tuning are presented in Table 2 and Table 4, respectively. We found that BART consistently outperforms other LLMs in both settings. We hypothesize that due to BART’s architectural nature as a denoising autoencoder, it is more suitable for translating natural language descriptions into executable action programs for the VirtualHome simulator.

**Different Environments** To test the performance variations under different environments, we conducted the experiments separately for each unique environment. The results are shown in Table 1 and Table 3, for fine-tuning SUM under IL and RL settings, respectively. Due to image observation variations having the most impact on SUM instead of APM, so we only test the performance of SUM under different environment settings. Through Table 1 and Table 3, we could find that the variations exist

among different environments. Generally, environment 6 seems to have the easiest environmental settings for the model to learn.

**Stability** To evaluate the stability of different models under different environments, we also calculated the standard deviation (stds) of the results across different trials. The results are shown in Tables 1,2,3,4, which shows that BART as APM and OFA seems to be more stable than the rest of the combinations.

**Analysis on the differences by different models and reasons** We found that the APM consistently generated high-quality executable actions and tasks based on metric scores. The primary reason for the substantial performance variations among models was the constraints within the environments. Each environment had predefined sets of actions, objects, and tasks. If the model generated items outside of these predefined distributions, the simulator couldn’t execute them. For example, the model might generate a valid action like  $[grab] < bottle > (1)$ , but if the “bottle” object wasn’t predefined in that environment, the simulator couldn’t execute the action. This environmental constraint led to the observed performance variations.

## 6 Conclusion

In this work, we introduce a novel robot learning paradigm with LLM in the loop that handles multiple modalities of visual observations and text-based actions in a principled manner. We bridge both modalities with natural language generated by a pretrained multimodal model. Our model contains SUM and APM, where SUM uses image observations as inputs taken by the robot to generate language descriptions of the current scene, and APM predicts the corresponding actions for the next step. We tested our method in the VirtualHome under 7 unique environments, and the results demonstrated that our proposed paradigm outperforms baselines in terms of execution rates and shows strong stability across environments. One interesting future direction is extending our proposed framework to solve generalization tasks in a more data and parameter-efficient manner.



## 7 Limitations.

- In our current study, we primarily focused on abstract high-level actions represented by language commands, without taking into account low-level controls such as joint motor control. This omission of the low-level control module may limit the overall effectiveness of the learned policies and their ability to function in complex and dynamic environments. An interesting future direction would be to consider the physical capabilities of embodied agents by learning universal low-level controllers for various morphologies.
- Our study might encounter challenges related to long-tailed actions. In our collected dataset, there are actions that occur infrequently, and the current method may not have effectively learned policies for scenarios involving such actions that rarely appear in the collected dataset. This limitation could constrain the overall effectiveness of the learned policies in real-world situations.
- Given that we fine-tuned the model using a dataset collected in the VirtualHome environment, the generalizability of the learned policies to other platforms might be insufficient due to significant differences between various simulated platforms.

## Acknowledgement

We greatly appreciate the valuable feedback from Lei Li, Christos Faloutsos, and Daniel Fried. This research is partially supported by CMU Computer Science Department fellowships.

## Code Availability

Our code is available at [https://github.com/Jason-Qiu/Embodied\\_Policy\\_Learning](https://github.com/Jason-Qiu/Embodied_Policy_Learning).

## References

- Michael Ahn et al. 2022. Do as i can, not as i say: Grounding language in robotic affordances. *ArXiv*, abs/2204.01691.
- Peter Anderson, Basura Fernando, Mark Johnson, and Stephen Gould. 2016. *SPICE: semantic propositional image caption evaluation*. *CoRR*, abs/1607.08822.

- Peter Anderson, Qi Wu, Damien Teney, Jake Bruce, Mark Johnson, Niko Sünderhauf, Ian D. Reid, Stephen Gould, and Anton van den Hengel. 2017. *Vision-and-language navigation: Interpreting visually-grounded navigation instructions in real environments*. *2018 IEEE/CVF Conference on Computer Vision and Pattern Recognition*, pages 3674–3683.
- Satanjeev Banerjee and Alon Lavie. 2005. Meteor: An automatic metric for mt evaluation with improved correlation with human judgments. In *IEE Evaluation@ACL*.
- Tom B. Brown et al. 2020. Language models are few-shot learners. *ArXiv*, abs/2005.14165.
- Arthur Fender C. Buckler, Luis F. C. Figueredo, Sami Haddadin, Ashish Kapoor, Shuang Ma, Sai Vemprala, and Rogerio Bonatti. 2022. Latte: Language trajectory transformer. *ArXiv*, abs/2208.02918.
- Kyunghyun Cho, Bart van Merriënboer, Çağlar Gülçehre, Dzmitry Bahdanau, Fethi Bougares, Holger Schwenk, and Yoshua Bengio. 2014. Learning phrase representations using rnn encoder–decoder for statistical machine translation. In *EMNLP*.
- Marcella Cornia, Matteo Stefanini, Lorenzo Baraldi, and Rita Cucchiara. 2019. Meshed-memory transformer for image captioning. *CVPR*, pages 10575–10584.
- Jacob Devlin, Ming-Wei Chang, Kenton Lee, and Kristina Toutanova. 2019. Bert: Pre-training of deep bidirectional transformers for language understanding. In *NAACL*.
- Jesse Dodge, Gabriel Ilharco, Roy Schwartz, Ali Farhadi, Hannaneh Hajishirzi, and Noah A. Smith. 2020. Fine-tuning pretrained language models: Weight initializations, data orders, and early stopping. *ArXiv*, abs/2002.06305.
- Linxi (Jim) Fan, Guanzhi Wang, Yunfan Jiang, Ajay Mandlkar, Yuncong Yang, Haoyi Zhu, Andrew Tang, De-An Huang, Yuke Zhu, and Anima Anandkumar. 2022. *Minedojo: Building open-ended embodied agents with internet-scale knowledge*. *ArXiv*, abs/2206.08853.
- Daniel Fried, Armen Aghajanyan, Jessy Lin, Sida I. Wang, Eric Wallace, Freda Shi, Ruiqi Zhong, Wen tau Yih, Luke Zettlemoyer, and Mike Lewis. 2022. Incoder: A generative model for code infilling and synthesis. *ArXiv*, abs/2204.05999.
- Samir Yitzhak Gadre, Mitchell Wortsman, Gabriel Ilharco, Ludwig Schmidt, and Shuran Song. 2022. Clip on wheels: Zero-shot object navigation as object localization and exploration. *ArXiv*, abs/2203.10421.
- Nishad Gothoskar, Miguel Lázaro-Gredilla, Abhishek Agarwal, Yasemin Bekiroglu, and Dileep George. 2020. Learning a generative model for robot control using visual feedback. *ArXiv*, abs/2003.04474.

- Kaiming He, Xiangyu Zhang, Shaoqing Ren, and Jian Sun. 2015. Deep residual learning for image recognition.
- Dan Hendrycks, Xiaoyuan Liu, Eric Wallace, Adam Dziedzi, R. Krishnan, and Dawn Xiaodong Song. 2020. Pretrained transformers improve out-of-distribution robustness. In *ACL*.
- Yicong Hong, Qi Wu, Yuankai Qi, Cristian Rodriguez-Opazo, and Stephen Gould. 2021. Vln-bert: A recurrent vision-and-language bert for navigation. *CVPR*, pages 1643–1653.
- Jeremy Howard and Sebastian Ruder. 2018. Universal language model fine-tuning for text classification. In *ACL*.
- Wenlong Huang, P. Abbeel, Deepak Pathak, and Igor Mordatch. 2022a. Language models as zero-shot planners: Extracting actionable knowledge for embodied agents. In *ICML*.
- Wenlong Huang, F. Xia, Ted Xiao, Harris Chan, Jacky Liang, Peter R. Florence, Andy Zeng, Jonathan Tompson, Igor Mordatch, Yevgen Chebotar, Pierre Sermanet, Noah Brown, Tomas Jackson, Linda Luu, Sergey Levine, Karol Hausman, and Brian Ichter. 2022b. [Inner monologue: Embodied reasoning through planning with language models](#). In *Conference on Robot Learning*.
- Yunfan Jiang, Agrim Gupta, Zichen Vincent Zhang, Guanzhi Wang, Yongqiang Dou, Yanjun Chen, Li Fei-Fei, Anima Anandkumar, Yuke Zhu, and Linxi (Jim) Fan. 2022. Vima: General robot manipulation with multimodal prompts. *ArXiv*, abs/2210.03094.
- Yash Kant et al. 2022. Housekeep: Tidying virtual households using commonsense reasoning. *ArXiv*, abs/2205.10712.
- Jared Kaplan et al. 2020. Scaling laws for neural language models. *ArXiv*, abs/2001.08361.
- Lei Ke, Wenjie Pei, Ruiyu Li, Xiaoyong Shen, and Yu-Wing Tai. 2019. Reflective decoding network for image captioning. *ICCV*, pages 8887–8896.
- Apoorv Khandelwal, Luca Weihs, Roozbeh Mottaghi, and Aniruddha Kembhavi. 2022. Simple but effective: Clip embeddings for embodied ai. *CVPR*, pages 14809–14818.
- Philipp Koehn. 2007. Statistical machine translation.
- Shuhei Kurita and Kyunghyun Cho. 2020. [Generative language-grounded policy in vision-and-language navigation with bayes’ rule](#). *ArXiv*, abs/2009.07783.
- Mike Lewis, Yinhan Liu, Naman Goyal, Marjan Ghazvininejad, Abdelrahman Mohamed, Omer Levy, Veselin Stoyanov, and Luke Zettlemoyer. 2020. Bart: Denoising sequence-to-sequence pre-training for natural language generation, translation, and comprehension. In *ACL*.
- Junnan Li, Dongxu Li, Caiming Xiong, and Steven Hoi. 2022a. Blip: Bootstrapping language-image pre-training for unified vision-language understanding and generation. *arXiv:2201.12086 [cs]*.
- Shuang Li, Xavier Puig, Yilun Du, Clinton Jia Wang, Ekin Akyürek, Antonio Torralba, Jacob Andreas, and Igor Mordatch. 2022b. Pre-trained language models for interactive decision-making. *ArXiv*, abs/2202.01771.
- Xiujun Li, Chunyuan Li, Qiaolin Xia, Yonatan Bisk, Asli Celikyilmaz, Jianfeng Gao, Noah A. Smith, and Yejin Choi. 2019. [Robust navigation with language pretraining and stochastic sampling](#). In *Conference on Empirical Methods in Natural Language Processing*.
- Xiujun Li et al. 2020. Oscar: Object-semantics aligned pre-training for vision-language tasks. In *ECCV*.
- J. Liang, Wenlong Huang, F. Xia, Peng Xu, Karol Hausman, Brian Ichter, Peter R. Florence, and Andy Zeng. 2022. Code as policies: Language model programs for embodied control. *ArXiv*, abs/2209.07753.
- Yuan-Hong Liao, Xavier Puig, Marko Boben, Antonio Torralba, and Sanja Fidler. 2019. [Synthesizing environment-aware activities via activity sketches](#).
- Bingqian Lin, Yi Zhu, Zicong Chen, Xiwen Liang, Jianzhao Liu, and Xiaodan Liang. 2022. Adapt: Vision-language navigation with modality-aligned action prompts. *CVPR*, pages 15375–15385.
- Chin-Yew Lin. 2004. Rouge: A package for automatic evaluation of summaries. In *ACL 2004*.
- Yinhan Liu, Myle Ott, Naman Goyal, Jingfei Du, Mandar Joshi, Danqi Chen, Omer Levy, Mike Lewis, Luke Zettlemoyer, and Veselin Stoyanov. 2019. Roberta: A robustly optimized bert pretraining approach. *ArXiv*, abs/1907.11692.
- Jiasen Lu, Dhruv Batra, Devi Parikh, and Stefan Lee. 2019. Vilbert: Pretraining task-agnostic visiolinguistic representations for vision-and-language tasks. In *Neural Information Processing Systems*.
- Yecheng Jason Ma et al. 2022. Vip: Towards universal visual reward and representation via value-implicit pre-training. *ArXiv*, abs/2210.00030.
- Arjun Majumdar, Ayush Shrivastava, Stefan Lee, Peter Anderson, Devi Parikh, and Dhruv Batra. 2020. Improving vision-and-language navigation with image-text pairs from the web. *ArXiv*, abs/2004.14973.
- Harry McGurk and John MacDonald. 1976. Hearing lips and seeing voices. *Nature*, 264:746–748.
- Abdalkarim Mohtasib, Gerhard Neumann, and Heriberto Cuayáhuitl. 2021. A study on dense and sparse (visual) rewards in robot policy learning. In *TAROS*.

- Van-Quang Nguyen, Masanori Suganuma, and Takayuki Okatani. 2022. Grit: Faster and better image captioning transformer using dual visual features. *ArXiv*, abs/2207.09666.
- Kishore Papineni, Salim Roukos, Todd Ward, and Wei-Jing Zhu. 2002. Bleu: a method for automatic evaluation of machine translation. In *ACL*.
- Simone Parisi, Aravind Rajeswaran, Senthil Purushwalkam, and Abhinav Kumar Gupta. 2022. The unsurprising effectiveness of pre-trained vision models for control. In *ICML*.
- Matthew E. Peters, Mark Neumann, Mohit Iyyer, Matt Gardner, Christopher Clark, Kenton Lee, and Luke Zettlemoyer. 2018. Deep contextualized word representations. In *NAACL*.
- Xavier Puig, Kevin Ra, Marko Boben, Jiaman Li, Tingwu Wang, Sanja Fidler, and Antonio Torralba. 2018a. Virtualhome: Simulating household activities via programs. *arXiv:1806.07011 [cs]*.
- Xavier Puig, Kevin Kyunghwan Ra, Marko Boben, Jiaman Li, Tingwu Wang, Sanja Fidler, and Antonio Torralba. 2018b. Virtualhome: Simulating household activities via programs. *CVPR*, pages 8494–8502.
- Jielin Qiu, Andrea Madotto, Zhaojiang Lin, Paul A Crook, Yifan Ethan Xu, Xin Luna Dong, Christos Faloutsos, Lei Li, Babak Damavandi, and Seungwhan Moon. 2024. Snapntell: Enhancing entity-centric visual question answering with retrieval augmented multimodal llm. *arXiv preprint arXiv:2403.04735*.
- Jielin Qiu, Jiacheng Zhu, Mengdi Xu, Franck Dernoncourt, Trung Bui, Zhaowen Wang, Bo Li, Ding Zhao, and Hailin Jin. 2023a. Sccs: Semantics-consistent cross-domain summarization via optimal transport alignment. In *Findings of the Association for Computational Linguistics: ACL 2023*, pages 1584–1601.
- Jielin Qiu, Yi Zhu, Xingjian Shi, Florian Wenzel, Zhiqiang Tang, Ding Zhao, Bo Li, and Mu Li. 2023b. Benchmarking robustness of multimodal image-text models under distribution shift. *Journal of Data-centric Machine Learning Research*.
- Alec Radford, Jong Wook Kim, Chris Hallacy, Aditya Ramesh, Gabriel Goh, Sandhini Agarwal, Girish Sastry, Amanda Askell, Pamela Mishkin, Jack Clark, Gretchen Krueger, and Ilya Sutskever. 2021. Learning transferable visual models from natural language supervision. In *ICML*.
- Colin Raffel, Noam M. Shazeer, Adam Roberts, Katherine Lee, Sharan Narang, Michael Matena, Yanqi Zhou, Wei Li, and Peter J. Liu. 2019. Exploring the limits of transfer learning with a unified text-to-text transformer. *ArXiv*, abs/1910.10683.
- Marc’Aurelio Ranzato, Sumit Chopra, Michael Auli, and Wojciech Zaremba. 2015. Sequence level training with recurrent neural networks. *CoRR*, abs/1511.06732.
- Allen Z. Ren, Bharat Govil, Tsung-Yen Yang, Karthik Narasimhan, and Anirudha Majumdar. 2022. Leveraging language for accelerated learning of tool manipulation. *ArXiv*, abs/2206.13074.
- Steven J. Rennie, Etienne Marcheret, Youssef Mroueh, Jerret Ross, and Vaibhava Goel. 2016. Self-critical sequence training for image captioning. *CVPR*, pages 1179–1195.
- Sebastian Ruder. 2021. Recent advances in language model fine-tuning.
- Nur Muhammad (Mahi) Shafiullah, Chris Paxton, Lerrel Pinto, Soumith Chintala, and Arthur D. Szlam. 2022. Clip-fields: Weakly supervised semantic fields for robotic memory. *ArXiv*, abs/2210.05663.
- Dhruv Shah, Blazej Osinski, Brian Ichter, and Sergey Levine. 2022. Lm-nav: Robotic navigation with large pre-trained models of language, vision, and action. *ArXiv*, abs/2207.04429.
- Mohit Shridhar, Lucas Manuelli, and Dieter Fox. 2021. Cliport: What and where pathways for robotic manipulation. *ArXiv*, abs/2109.12098.
- Mohit Shridhar, Lucas Manuelli, and Dieter Fox. 2022. Perceiver-actor: A multi-task transformer for robotic manipulation. *ArXiv*, abs/2209.05451.
- Ishika Singh, Valts Blukis, Arsalan Mousavian, Ankit Goyal, Danfei Xu, Jonathan Tremblay, Dieter Fox, Jesse Thomason, and Animesh Garg. 2022. **Prog-prompt: Generating situated robot task plans using large language models**. *2023 IEEE International Conference on Robotics and Automation (ICRA)*, pages 11523–11530.
- Kaitao Song, Xu Tan, Tao Qin, Jianfeng Lu, and Tie-Yan Liu. 2019. Mass: Masked sequence to sequence pre-training for language generation. *arXiv:1905.02450 [cs]*.
- Matteo Stefanini et al. 2021. From show to tell: A survey on deep learning-based image captioning. *IEEE Transactions on Pattern Analysis and Machine Intelligence*, 45:539–559.
- Nataliya Strokina, Wenyan Yang, Joni Pajarinen, Nikolay Serbenyuk, Joni-Kristian Kämäräinen, and Reza Ghahcheloo. 2022. Visual rewards from observation for sequential tasks: Autonomous pile loading. *Frontiers in Robotics and AI*, 9.
- Richard S Sutton, David McAllester, Satinder Singh, and Yishay Mansour. 1999. Policy gradient methods for reinforcement learning with function approximation. In *NeurIPS*, volume 12. MIT Press.
- Allison C. Tam et al. 2022. Semantic exploration from language abstractions and pretrained representations. *ArXiv*, abs/2204.05080.
- Hao Hao Tan and Mohit Bansal. 2019. Lxmert: Learning cross-modality encoder representations from transformers. *ArXiv*, abs/1908.07490.

- Kaisa Tiippana. 2014. What is the mcgurk effect? *Frontiers in Psychology*, 5.
- Ashish Vaswani, Noam Shazeer, Niki Parmar, Jakob Uszkoreit, Llion Jones, Aidan N Gomez, Lukasz Kaiser, and Illia Polosukhin. 2017a. Attention is all you need.
- Ashish Vaswani, Noam M. Shazeer, Niki Parmar, Jakob Uszkoreit, Llion Jones, Aidan N. Gomez, Lukasz Kaiser, and Illia Polosukhin. 2017b. Attention is all you need. *ArXiv*, abs/1706.03762.
- Ramakrishna Vedantam, C. Lawrence Zitnick, and Devi Parikh. 2015. Cider: Consensus-based image description evaluation. *arXiv:1411.5726 [cs]*.
- Jianfeng Wang, Xiaowei Hu, Pengchuan Zhang, Xiu-jun Li, Lijuan Wang, Lei Zhang, Jianfeng Gao, and Zicheng Liu. 2020. [Minivlm: A smaller and faster vision-language model](#). *CoRR*, abs/2012.06946.
- Peng Wang, An Yang, Rui Men, Junyang Lin, Shuai Bai, Zhikang Li, Jianxin Ma, Chang Zhou, Jingren Zhou, and Hongxia Yang. 2022. Unifying architectures, tasks, and modalities through a simple sequence-to-sequence learning framework. *arXiv:2202.03052 [cs]*.
- Zirui Wang, Jiahui Yu, Adams Wei Yu, Zihang Dai, Yulia Tsvetkov, and Yuan Cao. 2021. Simvlm: Simple visual language model pretraining with weak supervision. *arXiv:2108.10904 [cs]*.
- Ronald J. Williams. 1992. Simple statistical gradient-following algorithms for connectionist reinforcement learning. *Machine Learning*, 8:229–256.
- Ted Xiao, Harris Chan, Pierre Sermanet, Ayzaan Wahid, Anthony Brohan, Karol Hausman, Sergey Levine, and Jonathan Tompson. 2022. [Robotic skill acquisition via instruction augmentation with vision-language models](#). *ArXiv*, abs/2211.11736.
- Mengdi Xu, Yuchen Lu, Yikang Shen, Shun Zhang, Ding Zhao, and Chuang Gan. 2023. [Hyper-decision transformer for efficient online policy adaptation](#).
- Mengdi Xu, Yikang Shen, Shun Zhang, Yuchen Lu, Ding Zhao, Joshua Tenenbaum, and Chuang Gan. 2022. Prompting decision transformer for few-shot policy generalization. In *International Conference on Machine Learning*, pages 24631–24645. PMLR.
- B.P. Yuhas, M.H. Goldstein, and T.J. Sejnowski. 1989. [Integration of acoustic and visual speech signals using neural networks](#). *IEEE Communications Magazine*, 27:65–71.
- Rowan Zellers, Ari Holtzman, Matthew E. Peters, Roozbeh Mottaghi, Aniruddha Kembhavi, Ali Farhadi, and Yejin Choi. 2021. Piglet: Language grounding through neuro-symbolic interaction in a 3d world. In *ACL*.
- Andy Zeng, Adrian S. Wong, Stefan Welker, Krzysztof Choromanski, Federico Tombari, Aavek Purohit, Michael S. Ryoo, Vikas Sindhwani, Johnny Lee, Vincent Vanhoucke, and Peter R. Florence. 2022. [Socratic models: Composing zero-shot multimodal reasoning with language](#). *ArXiv*, abs/2204.00598.
- Pengchuan Zhang, Xiujun Li, Xiaowei Hu, Jianwei Yang, Lei Zhang, Lijuan Wang, Yejin Choi, and Jianfeng Gao. 2021. Vinvl: Revisiting visual representations in vision-language models. In *CVPR*, pages 5579–5588.
- Luowei Zhou, Hamid Palangi, Lei Zhang, Houdong Hu, Jason J. Corso, and Jianfeng Gao. 2019. Unified vision-language pre-training for image captioning and vqa. *ArXiv*, abs/1909.11059.
- Xizhou Zhu, Weijie Su, Lewei Lu, Bin Li, Xiaogang Wang, and Jifeng Dai. 2020. [Deformable DETR: deformable transformers for end-to-end object detection](#). *CoRR*, abs/2010.04159.



## A More Related Work

**Multimodal Learning** Formalized multimodal learning research dates back to 1989 when (Yuhas et al., 1989) conducted an experiment that built off the McGurk Effect for audio-visual speech recognition using neural networks (Tiippana, 2014; McGurk and MacDonald, 1976). Researchers in NLP and CV collaborated to make large and multimodal datasets available, catering to specific downstream tasks, such as classification, translation, and detection. In correlation, improvements in LLMs opened the gates to include other modalities of data, most frequently visual data (Wang et al., 2022; Qiu et al., 2023b; Nguyen et al., 2022; Li et al., 2022a; Wang et al., 2021; Qiu et al., 2023a; Shah et al., 2022; Zhang et al., 2021; Wang et al., 2020; Qiu et al., 2024). By utilizing the learned embeddings that have been pretrained on both language and image datasets, vision-language models are able to perform very well. Within the above success, image captioning has been an important task in multimodal learning, which aims at generating textual descriptions for the given images.

**Visual Feedback in Robot Learning** Visual feedback is commonly used in robot learning. Gothoskar et al. (2020) learned a generative model from actions to image observations of features to control a robot from visual feedback. Ma et al. (2022) proposed a self-supervised pretrained visual representation model which is capable of generating dense and smooth reward functions for unseen robotic tasks. Strokinina et al. (2022) reviewed the methods of reward estimation and visual representations used in learning-based approaches for robotics applications. Mohtasib et al. (2021) studied the performance of dense, sparse, visually dense, and visually sparse rewards in deep RL. Kurita and Cho (2020) proposed the direct navigation approach based on an image captioning model. Li et al. (2019) combined image captioning models and planning models, but Li et al. (2019) took pure language instructions as input, while our approach takes pure visual observations as input.

**Pre-training and Fine-tuning of Language Models** Over the past few years, fine-tuning (Howard and Ruder, 2018) has superseded the use of feature extraction of pretrained embeddings (Peters et al., 2018) while pretrained language models are favored over models trained on many tasks due to their increased sample efficiency and performance (Ruder, 2021). The success of these methods has led to the development of even larger models (Devlin et al., 2019; Raffel et al., 2019). But those large models may not perform well on data that is different from what they were pretrained on. Under this case, fine-tuning pretrained contextual word embedding models to supervised downstream tasks has become commonplace (Hendrycks et al., 2020; Dodge et al., 2020). Zeng et al. (2022) examined the sampling effects in reinforcement learning with GPT and BERT.

**Vision and Language Navigation** Anderson et al. (2017) proposed Vision-and-Language Navigation (VLN) as the problem of interpreting visually grounded navigation instructions. In Huang et al. (2022b), language instructions are utilized to interpret the scene, whereas we rely on raw image observations. In Singh et al. (2022), a predefined executable plan prompt is provided without learning from visual observations, simplifying the generation of executable plans. In Xiao et al. (2022), both language instructions and visual images are employed to fine-tune the VLM, which is subsequently used for behavior cloning. However, the generated robot plan consists of high-level natural language instructions rather than executable robot policies, as in our work. In Fan et al. (2022), the proposed MINECLIP primarily calculates the correlation between an open-vocabulary language goal string and a 16-frame video snippet. The correlation score serves as a learned dense reward function for training a robust multi-task RL agent, which is distinct from our approach.

**LLM Applications in Other Domains** Recently, LLMs have also shown great potential for accelerating learning in many other domains by generating learned embeddings as meaningful representations for downstream tasks and encoding transferable knowledge in large pretraining datasets. Examples include transferring the knowledge of LLM to, i.e., robotics control (Liang et al., 2022; Ahn et al., 2022), multimodal learning (Zeng et al., 2022; Zellers et al., 2021), decision-making (Li et al., 2022b; Huang et al., 2022a), code generation (Fried et al., 2022), laws (Kaplan et al., 2020), computer vision (Radford et al., 2021), and so on.

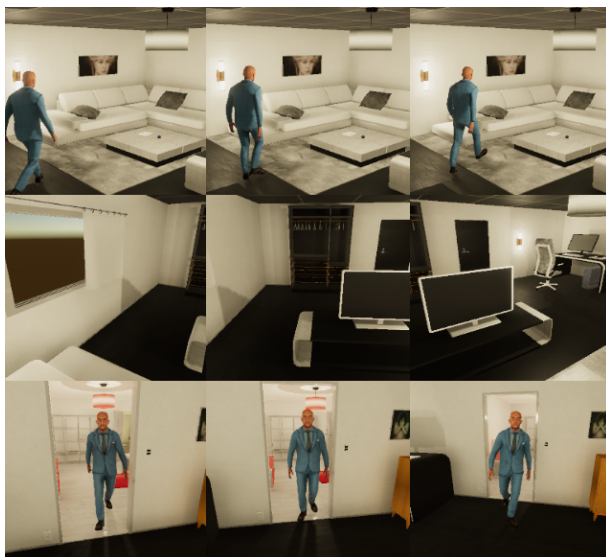


Figure 3: ‘AUTO’, ‘FIRST PERSON’, ‘FRONT PERSON’ views.

## B More Details of the Collected Dataset

**More details for data collection** During data collection, we utilized the VirtualHome simulator to collect visual and textual information about each action and overall task. For each task, it comprises of a series of actions and their corresponding objects like so:  $[[action_i] \langle object_i \rangle (id_i), \dots [action_n] \langle object_n \rangle (id_n)]$ , where  $i$  denotes each step of the task,  $action_i$  and  $object_i$  denotes the action performed on the object at step  $i$ , and  $id_i$  symbolizes the unique identifier of  $object_i$ . For each task, we would simulate it in VirtualHome and output each frame of the task as our visual observations. To conjure up the textual descriptions, we labeled each frame of the task with its corresponding  $[action_i] \langle object_i \rangle (id_i)$  (e.g., walk <bathroom> (1)). We then parsed this into a natural language format (e.g., walk <bathroom> (1) -> walk bathroom).

We noticed that the text descriptions were extremely short (e.g., walk bathroom, sitting chair, run treadmill). To create more informative and sensible textual descriptions, we applied prompt engineering by masking in between the action and object (i.e., walking [MASK] bathroom, sitting [MASK] chair, running [MASK] treadmill). This would then give us outputs such as walking **to** bathroom, sitting **on** chair, and running **on** treadmill.

For the finetuning of SUM, we input the visual observation (i.e., the frames gathered during data collection) and output an image caption that serves to describe the scene. We calculate the loss by utilizing the textual description we collected since these textual descriptions are supposed to represent the "action" being partaken during the frame.

**Divergence of text-image pairs and the number of the possible agent actions** The divergence of text-image pairs is in the different combinations of action and object pairs for each text-image pair. For example, let us say we have a task of “Turn on the Light”, and for this task, there are some actions, such as  $[[WALK] \langle bedroom \rangle (1), [WALK] \langle lamp \rangle (1), [SWITCHON] \langle lamp \rangle (1)]$ . For each action, there are  $N$  images (or frames) and text descriptions. For a given action, each image (frame) is different. However, for the text description, we simply use the same description as the ground truth for describing each image. Nevertheless, there is a diverse corpus of action-object combinations (we have 18 different actions and 308 different objects). In our study, there are 18 different actions, including [FIND], [TOUCH], [WALK], [SWITCHON], [GRAB], [READ], [STANDUP], [TURNTO], [LOOKAT], [SIT], [POINTAT], [OPEN], [WATCH], [RUN], [DRINK], [SWITCHOFF], [PUTOBJBACK], and [CLOSE].

## C Algorithms of Fine-tuning SUM and APM with Imitation Learning or REINFORCE

We provide the pseudo code for training SUM and APM in this section.

---

**Algorithm 1** Fine-tuning SUM

---

```
Initialize pretrained SUM model
Load VirtualHome dataset for fine-tuning
for  $n$  in num_epochs do
  for Image $_t$  and Caption $_t$  in batch $_n$  do
    1. Caption $_t = \text{SUM}(\text{Image}_t)$ 
    2. Loss $_{XE_t}(\theta_t) = L_{XE}(\text{Caption}_t, \hat{\text{Caption}}_t)$ 
    3.  $\theta_t \leftarrow \theta_t - \alpha \nabla_{\theta_t} L(\text{Caption}_t, \hat{\text{Caption}}_t)$ 
  end for
  repeat
    Steps 1 through 3
  until max(num_epochs) or convergence
end for
```

---

---

**Algorithm 2** Fine-tuning APM with Imitation Learning

---

```
Initialize fine-tuned SUM and pretrained APM
Load VirtualHome dataset for fine-tuning
for  $n$  in num_epochs do
  for Image $_t$ , Caption $_t$  Action $_t$  in batch $_n$  do
    1. Caption $_t = \text{SUM}(\text{Image}_t)$ 
    2. Action $_{t+1} = \text{APM}(\text{Caption}_t, \text{Action}_t)$ 
    3. Loss $_{XE_t}(\theta_t) = L_{XE}(\text{Action}_t, \hat{\text{Action}}_{t+1})$ 
    4.  $\theta_t \leftarrow \theta_t - \alpha \nabla_{\theta_t} L_{XE}(\text{Action}_t, \hat{\text{Action}}_{t+1})$ 
  end for
  repeat
    Steps 1 through 3
  until max(num_epochs) or convergence
end for
```

---

---

**Algorithm 3** Fine-tuning APM with REINFORCE

---

```
Initialize fine-tuned SUM, pretrained APM, and VirtualHome environment (env)
Load VirtualHome dataset for fine-tuning
for  $n$  in num_epochs do
  Trajectories $_t = []$ 
  state = env.reset()
  for Image $_t$ , Caption $_t$  Action $_t$  in batch $_n$  do
    1. Caption $_t = \text{SUM}(\text{Image}_t)$ 
    2. Action $_t = \text{APM}(\text{Caption}_t, \text{Action}_t)$ 
    3. Trajectories $_t.append(\text{Action}_t)$ 
  end for
  sort(Trajectories $_t$ ) by Task ID
  for  $i$  in range(len(Trajectories $_t$ )) do
    4. Action $_t = \text{sample\_action}(\text{Trajectories}_t[i])$ 
    5. Reward $_t = \text{env.step}(\text{Action}_t, \text{Action}_t)$ 
    6. Compute  $\nabla_{\theta_t} \log P(\text{Action}_t | \text{Action}_t)$ 
    7.  $\theta_t \leftarrow \theta_t + \alpha r \nabla_{\theta_t} \log P(\text{Action}_t | \text{Action}_t)$ 
  end for
  repeat
    Steps 1 through 7
  until max(num_epochs) or convergence
end for
```

---

## D Experimental Setup

**SUM Setting** For SUM, we use the following image captioning models to serve as SUM: OFA (Wang et al., 2022), BLIP (Li et al., 2022a), and GRIT (Nguyen et al., 2022). Both OFA and BLIP are pretrained on the same five datasets, while the GRIT model (Nguyen et al., 2022) is pretrained on a different combination of datasets. For OFA, we adopted OFA<sub>Large</sub> due to its superior performance in five variations. OFA<sub>Large</sub> wields ResNet152 (He et al., 2015) modules with 472M parameters and 12 encoders and decoder layers. For BLIP, we used ViT-L/16 as the image encoder due to its better performance. For GRIP, we follow Nguyen et al. (2022) which utilizes the Deformable DETR (Zhu et al., 2020) framework. Note that in our study we want SUM to generate captions that not only describe the scene but also try to derive action from it. We observe that adding the prompt "a picture of " following Wang et al. (2021) causes the model to be biased in solely describing the scene, which would in turn not be helpful for generating actionable captions. Therefore, we remove prompts in the SUM setting. We load pretrained models and fine-tune them for 7 epochs on our collected VirtualHome dataset. We keep the hyper-parameters consistent with the original implementations (Li et al., 2022a; Wang et al., 2022; Nguyen et al., 2022).

**APM Setting** We take LLM to act as the sole component in our APM. The goal of APM is to generate executable programs for the VirtualHome simulator. We deem the program outputted by the APM executable if the agent in the VirtualHome simulator is able to understand and perform the action. When the action is executed by the agent, the simulator is then directed to output images and captions that are

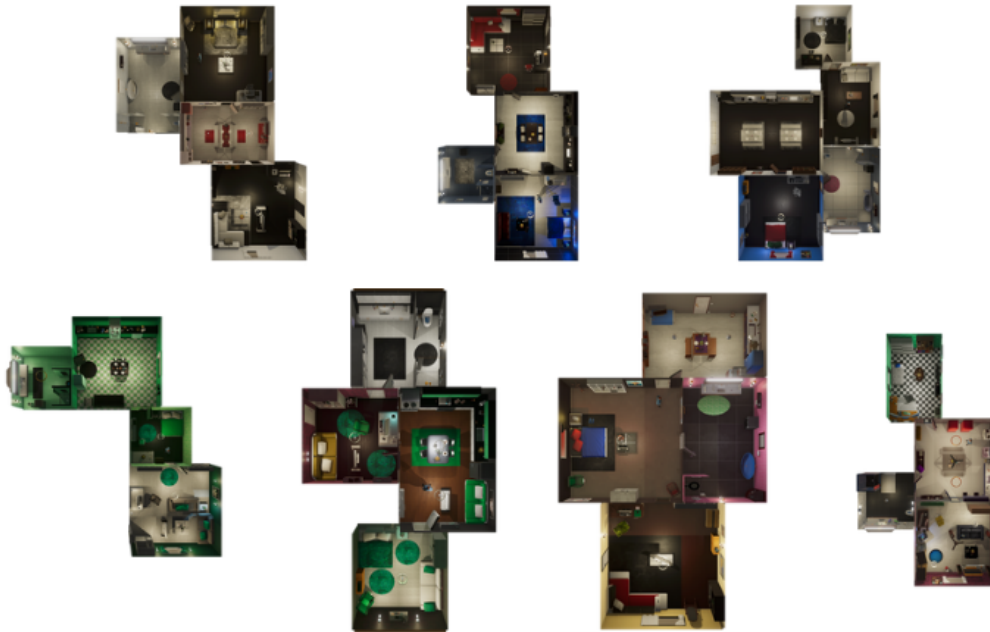


Figure 4: Top-down views of 7 different environments from VirtualHome.

synonymous with the input of SUM. The output hidden layers of SUM acts as the input embeddings to the APM, while the tokenized executable actions act as labels. The last hidden layer of APM acts as input embeddings for the tokenizer and generates token identifiers. The token identifiers are finally decoded into programmable actions that are fed into the VirtualHome simulator.

**Training and Testing Tasks** . We train and test on seven environments considering that in VirtualHome, there are seven environments in total. We use VirtualHome v0.1.0 due to its stability and to be consistent with previous works. We split the training and testing sets in terms of actions and tasks instead of environments (e.g., 20,000 actions in training and 3,000 in testing; 500 tasks in training, 200 in testing). We do this because each environment has different tasks and actions only executable in the given environment. The boundary between training and testing was chosen randomly based on the distribution of actions and tasks. As mentioned before, if there are a total of 10,000 different tasks or actions, we would randomly split the training and testing set to a proportion of 70:30, respectively. Unseen tasks are defined as tasks that are not included in the training set. For example, if we have the following example task of "Walk to the groceries" (e.g. [WALK] ⟨groceries⟩ (1)) in the training set, we would not have this task in the test set and vice versa.

**Executable Actions:** Here is the list of all actions executable in VirtualHome: [FIND, TOUCH, WALK, SWITCH ON, GRAB, READ, TURN TO, LOOK AT, SIT, POINT AT, OPEN, WATCH, RUN, DRINK, SWITCH OFF, PUT OBJECT BACK, CLOSE, STAND UP].

## E More Experimental Results

**Fine-tuning performance on in-distribution tasks and unseen tasks** To further support our findings, we conducted additional experiments that tested the fine-tuning performance on in-distribution tasks and unseen tasks in the VirtualHome environment following the setting in Li et al. (2022b). Li et al. (2022b) used reinforcement learning to adapt to downstream tasks. It’s important to note that Li et al. (2022b) used oracle text-based inputs that summarize the current observation, whereas we use raw image inputs and understand the scene with our fine-tuned SUM module. We measure the performance with the episode success rate and summarize the main comparison results with Li et al. (2022b) in Table 5. Our results show that when fine-tuning with REINFORCE, our method outperforms Li et al. (2022b) in both in-distribution tasks and novel tasks. Additionally, when expert data is available in the downstream tasks, fine-tuning with imitation learning outperforms the REINFORCE approach.



Table 5: Comparison of episode success rate.

| Method                    | In-Distribution Tasks | Novel Tasks |
|---------------------------|-----------------------|-------------|
| Li et al. (2022b)         | 53.7                  | 27.8        |
| Ours (REINFORCE)          | 58.4                  | 33.7        |
| Ours (Imitation Learning) | 68.4                  | 44.8        |

Table 6: Our fine-tuning results for different SUM/APM configurations in in-distribution and novel tasks, as well as using REINFORCE and imitation learning strategies. We measure the performance based on the episode success rate.

| SUM  | APM     | In-Distribution REINFORCE | Novel Tasks REINFORCE | In-Distribution Imitation | Novel Tasks Imitation |
|------|---------|---------------------------|-----------------------|---------------------------|-----------------------|
| OFA  | BERT    | 56.1                      | 31.4                  | 65.2                      | 40.7                  |
|      | BART    | <b>58.4</b>               | <b>33.7</b>           | <b>68.4</b>               | <b>44.8</b>           |
|      | RoBERTa | 51.7                      | 32.3                  | 66.0                      | 42.8                  |
| BLIP | BERT    | 53.7                      | 28.5                  | 61.1                      | 39.5                  |
|      | BART    | 55.2                      | 31.2                  | 64.3                      | 40.3                  |
|      | RoBERTa | 50.6                      | 29.3                  | 62.8                      | 39.8                  |
| GRIT | BERT    | 50.5                      | 28.8                  | 61.3                      | 40.4                  |
|      | BART    | 51.2                      | 30.0                  | 63.7                      | 39.6                  |
|      | RoBERTa | 49.0                      | 27.1                  | 59.2                      | 38.7                  |

**Importance and necessity of fine-tuning** To underscore the importance and necessity of fine-tuning, we present additional zero-shot testing performances without fine-tuning in Table 7 and Table 8. Our findings reveal that the episode success rate and action execution rates are significantly lower without fine-tuning in both methods, which highlights the crucial role that fine-tuning plays in improving performance.

**How Visual Observations Affect SUM** The quality of visual observations has an important effect on SUM. For a view like FIRST\_PERSON, where the camera’s perspective is in first person, we noticed that since this view does not explicitly show the agent performing some actions, it was harder for our SUM model to generate high-quality textual descriptions. Another example is the complexity of the visual observation. For example, we found some images of a blank wall or, on the contrary, a very dense observation with many different objects. For such cases, we found that SUM could not generate informative descriptions that fit the action or task being performed.

**Analysis on the differences by different models and reasons** During evaluation, we tested our models with 10 different seeds to ensure robustness and reported the mean and standard deviations for all models and environments. As per Table 1, it is important to note that the standard deviations for execution rate across all three models are generally pretty high (i.e.,  $\pm 0.93$  -  $\pm 5.98$ ). We observed that the executable actions and overall tasks generated by the APM were of high quality (as per the BLEU, ROUGE, METEOR, CIDEr, and SPICE scores). We found that the most significant attribute to the high variations in performances was the environment’s constraints. Each environment has a predefined, finite number of actions, objects, and tasks. Therefore, if our model generated some actions, objects, or tasks that are not within the distribution, the simulator would not be able to execute them. For example, our model would generate a sensible action such as  $[grab] < bottle > (1)$  in environment 1. However, in this environment, the bottle object was not predefined, thus preventing the simulator from executing the action. This characteristic led to the high variations of the performance across models. We acknowledge that this bottleneck is important and hope to consider it in future works.

## F Experiment Parameters

In this section, we listed the experimental parameters in Tables 9, 10, and 11.

## G Markov Decision Processes

**Markov decision process.** A Markov decision process (MDP) is defined as a 5-tuple  $(\mathcal{S}, \mathcal{A}, T, R, \gamma)$ , where  $\mathcal{S}$  and  $\mathcal{A}$  are the state and action space, respectively. In our situation, the states are the visual

Table 7: Comparison action execution rates in zero-shot and fine-tuned settings using both REINFORCE and Imitation Learning.

| Method | APM        | SUM        | REINFORCE | Imitation Learning |
|--------|------------|------------|-----------|--------------------|
| 1      | Zero-shot  | Zero-shot  | 0.1       | 0.1                |
| 2      | Zero-shot  | Fine-tuned | 14.5      | 21.4               |
| 3      | Fine-tuned | Zero-shot  | 5.8       | 6.9                |
| 4      | Fine-tuned | Fine-tuned | 57.2      | 77.8               |

Table 8: Comparison episode success rate in zero-shot and fine-tuned settings using both REINFORCE and Imitation Learning.

| Method | APM        | SUM        | REINFORCE | Imitation Learning |
|--------|------------|------------|-----------|--------------------|
| 1      | Zero-shot  | Zero-shot  | 0.7       | 0.7                |
| 2      | Zero-shot  | Fine-tuned | 16.7      | 19.5               |
| 3      | Fine-tuned | Zero-shot  | 7.7       | 8.7                |
| 4      | Fine-tuned | Fine-tuned | 58.4      | 76.8               |

Table 9: Experiment parameters used in SUMs, where the best ones are marked in bold.

| SUM  | Batch Size              | Encoder Layers | Att. Heads    | Learning Rate               | Dropout                  | Epochs                     |
|------|-------------------------|----------------|---------------|-----------------------------|--------------------------|----------------------------|
| OFA  | [4, <b>8</b> , 16, 32]  | [ <b>24</b> ]  | [ <b>16</b> ] | [1e-4, <b>1e-5</b> , 1e-7]  | [ <b>0.1</b> , 0.2, 0.3] | [2, 5, <b>10</b> , 20, 50] |
| BLIP | [8, 16, <b>32</b> , 64] | [ <b>12</b> ]  | [ <b>12</b> ] | [1e-4, <b>1e-5</b> , 1e-7]  | [0.1, 0.2, <b>0.3</b> ]  | [2, <b>5</b> , 10, 20, 50] |
| GRIT | [4, 8, 16, <b>32</b> ]  | [ <b>6</b> ]   | [ <b>8</b> ]  | [ <b>1e-4</b> , 1e-5, 1e-6] | [0.1, <b>0.2</b> , 0.3]  | [2, 5, <b>10</b> , 20, 50] |

Table 10: Experiment parameters used in Supervised APMs, where the best ones are marked in bold

| APM     | Batch Size              | Encoder Layers | Att. Heads    | Learning Rate               | Dropout                 | Epochs                     |
|---------|-------------------------|----------------|---------------|-----------------------------|-------------------------|----------------------------|
| BERT    | [4, <b>8</b> , 16, 32]  | [ <b>12</b> ]  | [ <b>12</b> ] | [1e-4, <b>1e-5</b> , 1e-7]  | [0.1, 0.2, <b>0.3</b> ] | [2, 5, <b>10</b> , 20, 50] |
| BART    | [8, 16, <b>32</b> , 64] | [ <b>12</b> ]  | [ <b>16</b> ] | [1e-4, <b>1e-5</b> , 1e-7]  | [0.1, 0.2, <b>0.3</b> ] | [2, 5, <b>10</b> , 20, 50] |
| RoBERTa | [4, 8, 16, <b>32</b> ]  | [ <b>12</b> ]  | [ <b>12</b> ] | [ <b>1e-4</b> , 1e-5, 1e-7] | [0.1, 0.2, <b>0.3</b> ] | [2, 5, <b>10</b> , 20, 50] |

Table 11: Experiment parameters used in REINFORCE APMs, where the best ones are marked in bold

| APM     | Batch Size              | Encoder Layers | Att. Heads    | Learning Rate              | Dropout                 | Epochs                     |
|---------|-------------------------|----------------|---------------|----------------------------|-------------------------|----------------------------|
| BERT    | [4, <b>8</b> , 16, 32]  | [ <b>12</b> ]  | [ <b>12</b> ] | [1e-4, <b>1e-5</b> , 1e-7] | [0.1, 0.2, <b>0.3</b> ] | [2, 5, <b>10</b> , 20, 50] |
| BART    | [8, 16, <b>32</b> , 64] | [ <b>12</b> ]  | [ <b>16</b> ] | [1e-4, <b>1e-5</b> , 1e-7] | [0.1, 0.2, <b>0.3</b> ] | [2, 5, <b>10</b> , 20, 50] |
| RoBERTa | [4, 8, 16, <b>32</b> ]  | [ <b>12</b> ]  | [ <b>12</b> ] | [1e-4, <b>1e-5</b> , 1e-7] | [0.1, <b>0.2</b> , 0.3] | [2, 5, <b>10</b> , 20, 50] |

observations  $V$ .  $T : \mathcal{S} \times \mathcal{A} \rightarrow \Delta(\mathcal{S})$  is the transition function,  $R : \mathcal{S} \times \mathcal{A} \rightarrow \mathbb{R}$  is the reward function, and  $\gamma$  is the discount factor. We consider a sparse reward setting and assume the  $\gamma = 1$ . We aim to find an optimal policy  $\pi =: \mathcal{S} \rightarrow \mathcal{A}$  that maximizes the expected return  $\mathbb{E}_{\tau \sim \pi} \left[ \sum_{t=0}^{H-1} \gamma^t r(s_t, a_t) \right]$ .  $H$  is the episode length.